J. Fluid Mech. (1998), *vol.* 363, *pp.* 333–347. Printed in the United Kingdom

An operator expansion formalism for nonlinear surface waves over variable depth

By RALPH A. SMITH

Areté Associates, Sherman Oaks, CA 91413-6024, USA

(Received 29 October 1997 and in revised form 30 January 1998)

The Hamiltonian formalism for surface waves associated with the method of Watson & West (1975) is extended to handle the case of spatially varying bottom depth. This description models moderately nonlinear waves over a wider range of scales than Boussinesq-type approximations. A pseudospectral simulation code has been developed using this formalism in two horizontal dimensions. Computations using the model compare well with measurements of waves over a bar, diffractive focusing by topography, and shoaling of solitary waves. Waveforms are computed accurately until near the point of breaking.

1. Introduction

Accurate modelling of surface wave dynamics in coastal regions has been the goal of much recent research, which has been summarized in surveys by Mei & Liu (1993), Dingemans (1997), and Kirby (1997). The richness of coastal wave dynamics arises from the large amplitudes of the waves and the wide variations in depth. The interplay of the resulting refraction, diffraction, and nonlinear wave interaction is most often treated by approximations of the Boussinesq type. Such models are valid when the wavelengths are long compared to the local depth, but misrepresent the dispersion and harmonic content of shorter waves.

The subject of the present work is an alternative description which simultaneously captures both short and long waves of moderate amplitude, and which affords a means for efficient and accurate computation. This approach is based on a Hamiltonian formalism using the expansion method of Watson & West (1975), which has been fruitful in studies of deep-water waves. An advantage of Hamiltonian formulations is their clear manifestation of conservation laws. The Boussinesq equations and related dynamical models can be expressed in terms of Hamiltonians, as shown by Mooiman (1991), Yoon & Liu (1994), and Dingemans (1997). Radder (1992) and Choi (1995) have expressed surface wave dynamics using other Hamiltonian formulations, without a shallow-water approximation. The latter models differ in both analytic and computational details from the present scheme. Wright & Creamer (1994) studied the eikonal limit of a Hamiltonian description similar to the following. The formalism developed here is well suited to numerical work, and may also be useful for analytic studies of nonlinear wave interactions in the presence of non-trivial topography. It is most closely related to the Dirichlet–Neumann formalism of Craig & Sulem (1993), whose connection to other shallow-water models has been discussed by Craig & Groves (1994).

In the next section, I review the operator expansion formalism and extend it to finite, varying depth. I then discuss some limiting cases and other properties of the formalism. Some results of computer simulations based on the new formalism are then presented. These demonstrate that the scheme is accurate for a variety of problems involving wave nonlinearity, shoaling, and diffraction. This study is limited to mild bottom slopes; further analysis of the approximations used here, including limitations on bottom roughness, will be presented elsewhere.

2. Operator expansion formalism

We begin with a Hamiltonian formulation of surface-wave dynamics involving irrotational flow in an incompressible, inviscid fluid. The Hamiltonian formulation is due to Zakharov (1968), Broer (1974), and Miles (1977); the operator version used here was introduced by Milder (1977). I employ the methods of Watson & West (1975), and notation similar to that of Milder (1990). The kinematic and dynamical boundary conditions on surface height $\zeta(\boldsymbol{x}, t)$ and surface potential $\phi(\boldsymbol{x}, t)$, specified as functions of horizontal Cartesian coordinates $\boldsymbol{x}$, are

$$\frac{\partial \zeta}{\partial t} + \nabla\phi \cdot \nabla\zeta = w[1 + (\nabla\zeta)^2], \tag{2.1}$$

$$\frac{\partial \phi}{\partial t} = \frac{1}{2} w^2 [1 + (\nabla\zeta)^2] - \tfrac{1}{2}(\nabla\phi)^2 - g\zeta, \tag{2.2}$$

where ∇ is the horizontal gradient and g is gravitational acceleration. The vertical velocity w is determined from ϕ by a non-local linear operator ($w = \mathbf{D}\phi$), which is described in detail below. The fields ζ and ϕ are a canonically conjugate pair for the Hamiltonian

$$H = \frac{1}{2} \int \left(\phi \mathbf{K} \phi + g\zeta^2\right) \mathrm{d}\boldsymbol{x}, \tag{2.3}$$

where the normal differential operator is defined by

$$\mathbf{K} = [1 + (\nabla\zeta)^2]\mathbf{D} - (\nabla\zeta) \cdot \nabla. \tag{2.4}$$

We proceed by developing $\mathbf{D}$ and $\mathbf{K}$ as operator series in powers of ζ and of the depth deviation from a constant value. When H is truncated at a given order, the canonical equations

$$\frac{\partial \zeta}{\partial t} = \frac{\delta H}{\delta \phi} \quad \text{and} \quad \frac{\partial \phi}{\partial t} = -\frac{\delta H}{\delta \zeta} \tag{2.5}$$

constitute a consistent dynamical model, which enjoys the properties (and shortcomings) described by Milder (1990). In particular, nonlinear wave–wave interactions are described quite accurately. This scheme has been used for simulations of waves on deep water, as described by West *et al.* (1987).

2.1. *Expansion of the vertical derivative*

It remains to specify a useful form for the operator $\mathbf{D}$. The surface potential ϕ is the restriction of a volume potential $\Phi(\boldsymbol{x}, z)$ to the surface $z = \zeta(\boldsymbol{x})$. Let $\phi_0(\boldsymbol{x})$ denote the potential at $z = 0$. Let the bottom of the fluid region be defined by

$$z = -h(\boldsymbol{x}) = -h_0 - \delta h(\boldsymbol{x}), \tag{2.6}$$

where h_0 is a constant reference depth. Suppose that Φ is sufficiently smooth to have a well-behaved Fourier expansion. Let $F(\boldsymbol{x}, z; h)$ denote the solution of

$$\left.\begin{aligned} (\nabla^2 + \partial_z^2)F &= 0, \\ F(\boldsymbol{x}, 0) &= \phi_0(\boldsymbol{x}), \\ \partial_z F + \nabla h \cdot \nabla F &= 0 \quad \text{at} \quad z = -h. \end{aligned}\right\} \tag{2.7}$$

Then for smooth

$$\phi_0(\boldsymbol{x}) = \int \mathrm{d}\boldsymbol{k}\, \mathrm{e}^{\mathrm{i}\boldsymbol{k}\cdot\boldsymbol{x}} f(\boldsymbol{k}), \tag{2.8}$$

where $\boldsymbol{k} = \boldsymbol{k}/(2\pi)^2$, we have

$$F(\boldsymbol{x}, z; h_0) = \int \mathrm{d}\boldsymbol{k}\, \mathrm{e}^{\mathrm{i}\boldsymbol{k}\cdot\boldsymbol{x}} \frac{\cosh k(z + h_0)}{\cosh k h_0} f(\boldsymbol{k}). \tag{2.9}$$

If the potential is decomposed according to

$$\Phi = F(\boldsymbol{x}, z; h) = F(\boldsymbol{x}, z; h_0) + \delta F(\boldsymbol{x}, z), \tag{2.10}$$

then δF is a potential satisfying the boundary conditions

$$\left.\begin{aligned} \delta F &= 0 \quad \text{at} \quad z = 0, \\ (\partial_z + \nabla \delta h \cdot \nabla)\delta F &= -(\partial_z + \nabla \delta h \cdot \nabla) F(h_0) \quad \text{at} \quad z = -h, \end{aligned}\right\} \tag{2.11}$$

so it has the expansion

$$\delta F(\boldsymbol{x}, z) = \int \mathrm{d}\boldsymbol{k}\, \mathrm{e}^{\mathrm{i}\boldsymbol{k}\cdot\boldsymbol{x}} \frac{\sinh kz}{\cosh k h_0} \delta f(\boldsymbol{k}). \tag{2.12}$$

The coefficients $\delta f(\boldsymbol{k})$ may be computed from the boundary condition:

$$\begin{aligned} &\int \mathrm{d}\boldsymbol{k}\, \mathrm{e}^{\mathrm{i}\boldsymbol{k}\cdot\boldsymbol{x}} \big[k(\cosh k\delta h + \tanh k h_0 \sinh k\delta h) \\ &\qquad -\mathrm{i}(\nabla\delta h)\cdot\boldsymbol{k}(\tanh k h_0 \cosh k\delta h + \sinh k\delta h)\big]\, \delta f(\boldsymbol{k}) \\ &= \int \mathrm{d}\boldsymbol{k}\, \mathrm{e}^{\mathrm{i}\boldsymbol{k}\cdot\boldsymbol{x}} \big[k \operatorname{sech} k h_0 \sinh k\delta h \\ &\qquad - \mathrm{i}(\nabla\delta h)\cdot\boldsymbol{k} \operatorname{sech} k h_0 \cosh k\delta h\big] f(\boldsymbol{k}). \end{aligned} \tag{2.13}$$

Equation (2.13) is exact. For moderate values of $\delta h/h_0$, it may be solved by iteration. The presence of $\operatorname{sech} k h_0$ in the operators on the right-hand side makes the approximation good even for large $k\delta h$. For future reference, it will be convenient to define an operator $\mathbf{H}$ by the solution of (2.13):

$$\int \mathrm{d}\boldsymbol{k}\, \mathrm{e}^{\mathrm{i}\boldsymbol{k}\cdot\boldsymbol{x}} \delta f(\boldsymbol{k}) \operatorname{sech} k h_0 = \mathbf{H} \int \mathrm{d}\boldsymbol{k}\, \mathrm{e}^{\mathrm{i}\boldsymbol{k}\cdot\boldsymbol{x}} f(\boldsymbol{k}) \equiv \mathbf{H}\phi_0(\boldsymbol{x}). \tag{2.14}$$

To second order in δh, it is given by

$$\begin{aligned} \mathbf{H} \sim (\operatorname{sech} k h_0)_{\mathrm{op}}\, \mathbf{k}^{-1} &\left[1 - \delta h\, (k \tanh k h_0)_{\mathrm{op}} + (\nabla\delta h)\cdot\nabla \left(k^{-1} \tanh k h_0\right)_{\mathrm{op}}\right] \\ &\times [\delta h \mathbf{k}^2 - (\nabla\delta h)\cdot\nabla]\, (\operatorname{sech} k h_0)_{\mathrm{op}} \end{aligned} \tag{2.15}$$

$$= -(\operatorname{sech} k h_0)_{\mathrm{op}}\, \mathbf{k}^{-1} [1 + \nabla\cdot\delta h\, \nabla \left(k^{-1} \tanh k h_0\right)_{\mathrm{op}}] \nabla\cdot\delta h\, \nabla\, (\operatorname{sech} k h_0)_{\mathrm{op}}\,. \tag{2.16}$$

Here and in the following we make use of pseudodifferential operators denoted by their representation in wavenumber space:

$$(a(k))_{\mathrm{op}}\, f(\boldsymbol{x}) = \int \mathrm{d}\boldsymbol{k}\, \mathrm{d}\boldsymbol{x}' \mathrm{e}^{\mathrm{i}\boldsymbol{k}\cdot(\boldsymbol{x}-\boldsymbol{x}')} a(k) f(x'), \tag{2.17}$$

and $\mathbf{k}^p = (k^p)_{\mathrm{op}}$,

Following Milder, I introduce a vertical differential operator which maps ϕ_0 into the vertical velocity on the mean plane:

$$\mathbf{D}_0 \phi_0(\boldsymbol{x}) = \partial_z \Phi(\boldsymbol{x}, z = 0). \tag{2.18}$$

By direct substitution, we find that

$$\begin{aligned} \mathbf{D}_0 &= (k \tanh kh_0)_{\mathrm{op}} + \mathbf{kH} \\ &\sim (k \tanh kh_0)_{\mathrm{op}} - (\operatorname{sech} kh_0)_{\mathrm{op}} \nabla \cdot \delta h \nabla (\operatorname{sech} kh_0)_{\mathrm{op}}. \end{aligned} \tag{2.19}$$

2.2. *Extension to finite-amplitude waves*

Next we extend the vertical differential operator up to an interface at $z = \zeta(\boldsymbol{x})$. The potential on the interface is

$$\begin{aligned} \phi(\boldsymbol{x}) &= \Phi\Big(\boldsymbol{x}, \zeta(\boldsymbol{x})\Big) \\ &= \int \mathrm{d}\boldsymbol{k}\, \mathrm{e}^{\mathrm{i}\boldsymbol{k}\cdot\boldsymbol{x}} [f(\boldsymbol{k})(\cosh k\zeta + \sinh k\zeta\, \tanh kh_0) + \delta f(\boldsymbol{k}) \sinh k\zeta \operatorname{sech} kh_0] \\ &= [(\cosh k\zeta)_{\mathrm{op}} + (\sinh k\zeta\, \tanh kh_0)_{\mathrm{op}} + (\sinh k\zeta)_{\mathrm{op}} \mathbf{H}]\phi_0, \end{aligned} \tag{2.20}$$

where operators such as $(\cosh k\zeta)_{\mathrm{op}}$ are defined by an operator series expansion in which pointwise multiplication by powers of ζ occurs after application of the appropriate Fourier space operator:

$$(\cosh k\zeta)_{\mathrm{op}} = \sum_{n=0}^{\infty} \frac{1}{(2n)!} \zeta^{2n} \mathbf{k}^{2n}. \tag{2.21}$$

The vertical velocity component at the interface is

$$\mathbf{D}\phi = [(\cosh k\zeta\, k \tanh kh_0 + \sinh k\zeta\, k)_{\mathrm{op}} + (\cosh k\zeta\, k)_{\mathrm{op}} \mathbf{H}]\phi_0. \tag{2.22}$$

We can invert the operator equation (2.20) iteratively:

$$\phi_0 \sim \phi - \zeta\, (k \tanh kh_0)_{\mathrm{op}}\, \phi - \zeta \mathbf{kH}\phi - \tfrac{1}{2}\zeta^2 \mathbf{k}^2 \phi + [\zeta \mathbf{k}((\tanh kh_0)_{\mathrm{op}} + \mathbf{H})]^2 \phi. \tag{2.23}$$

Let us introduce the operator

$$\mathbf{H}' = (\tanh kh_0)_{\mathrm{op}} + \mathbf{H}. \tag{2.24}$$

Then the operator $\mathbf{D}$ to second order in ζ is

$$\mathbf{D}\phi \sim \mathbf{kH}'\phi + [\zeta \mathbf{k}^2 - \mathbf{kH}'\zeta \mathbf{kH}']\phi + [-\zeta \mathbf{k}^2 \zeta \mathbf{kH}' - \tfrac{1}{2}\mathbf{kH}'\zeta^2 \mathbf{k}^2 + \tfrac{1}{2}\zeta^2 \mathbf{k}^3 \mathbf{H}' + \mathbf{kH}'(\zeta \mathbf{kH}')^2]\phi. \tag{2.25}$$

In the case of two-dimensional waves over uniform depth, (2.25) leads to the model of Craig & Sulem (1993), as I show in the Appendix.

In the deep water limit, $\mathbf{H}'$ becomes the identity operator, so we have

$$\lim_{h_0 \to \infty} \mathbf{D} \sim \mathbf{k} + \zeta \mathbf{k}^2 - \mathbf{k}\zeta \mathbf{k} - \zeta \mathbf{k}^2 \zeta \mathbf{k} - \tfrac{1}{2}\mathbf{k}\zeta^2 \mathbf{k}^2 + \tfrac{1}{2}\zeta^2 \mathbf{k}^3 + \mathbf{k}\zeta \mathbf{k}\zeta \mathbf{k}, \tag{2.26}$$

which coincides with Milder's formula.

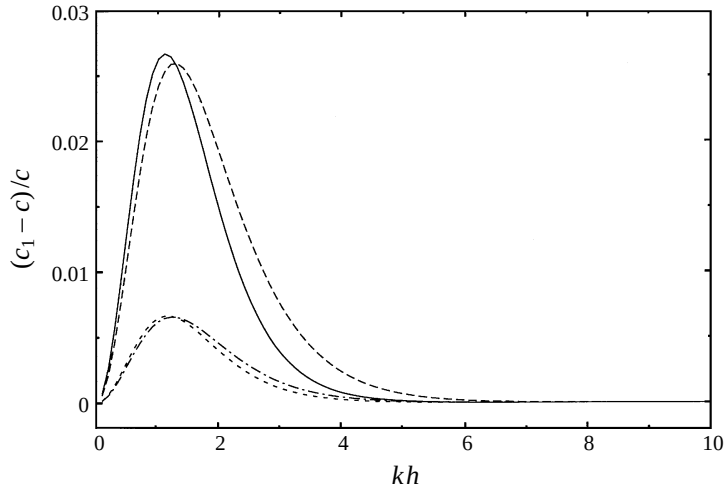

FIGURE 1. Fractional errors in phase speed over constant depth: c_1 is the phase speed obtained from (2.19) with constant δh; c is the true value obtained from (3.3). Solid line: $h = 1.414h_0$; dashed line: $h = 0.707h_0$; dotted line: $h = 1.189h_0$; chained line: $h = 0.84h_0$.

3. Properties of the model

Small-amplitude surface waves are described by the system

$$\partial_t \phi_0 + g\zeta = 0, \quad \partial_t \zeta - \mathbf{D}_0 \phi_0 = 0. \tag{3.1}$$

Thus linear surface waves evolve according to the equation

$$\partial_t^2 \phi_0 + g\mathbf{D}_0 \phi_0 = 0. \tag{3.2}$$

For a level bottom at depth h_0, this is equivalent to the physically correct dispersion relation

$$\omega^2 = gk \tanh kh_0. \tag{3.3}$$

For a constant depth h not equal to the reference depth h_0, the above formalism approximates the linear wave dispersion relation by a Taylor series in δh. This differs from the Boussinesq approximation, which involves an expansion in h itself. Hence the new description can be more accurate than the Boussinesq approximation for waves in the regime $kh > 1$. Figure 1 shows the fractional errors in phase speed associated with the operator expansion truncated at first order in δh (i.e. that given by (2.19) with constant δh), as a function of kh. If the range of depths is sufficiently large, interpolation among multiple reference depths further improves the accuracy. Details of such an interpolation scheme are discussed below. The Hamiltonian formulation, in combination with the adiabatic invariance of wave action, ensures that accuracy of dispersion leads to similar accuracy of linear shoaling coefficients, which are awkward to express analytically.

In the limit of small h_0 and moderate bottom slopes, the operator expansion dynamics are asymptotically equivalent to Airy's shallow-water equations. Specifically, upon taking $h_0 = 0$ and retaining terms of first order in δh and second order in ζ, we have

$$\frac{\partial \zeta}{\partial t} + \nabla \cdot [\boldsymbol{u}(\zeta + \delta h)] = O(\delta h^2, \zeta^3), \tag{3.4}$$

$$\frac{\partial \boldsymbol{u}}{\partial t} + \boldsymbol{u} \cdot \nabla \boldsymbol{u} + g \nabla \zeta = O(\delta h^2, \zeta^3), \tag{3.5}$$

where $\boldsymbol{u} = \nabla \phi$. This model is widely used to describe very long-wavelength phenomena.

The operator expansion may be interpreted as a slope expansion of the resolvent of a boundary integral operator of potential theory; Milder (1996) presented details of such an interpretation in the related context of the Helmholtz equation. This suggests that the expansion in (2.16) should be useful for bottom slopes up to nearly unity. An analysis of how accuracy depends on topography will be presented elsewhere. The method is unable to reach similarly large surface slopes for dynamical reasons.

The truncated Hamiltonian, like the deep-water one of Milder (1990), is not, in general, positive definite. More precisely, the second variation $\delta^2 H\{\zeta_0, \phi_0\}$ around a reference solution ζ_0, ϕ_0 may have negative eigenvalues when ζ_0 is sufficiently complicated. This is not a problem for small-amplitude waves around the still-water equilibrium; as mentioned above, linear waves over uniform depth obey the correct dispersion relation for all wavelengths. Moreover, the studies of waves of moderate amplitude discussed below have not been afflicted by this failure. However, when there are very steep long waves, and if much shorter waves are included in a simulation, the non-physical short-wavelength instability described by Milder arises. When the short-wave amplitudes also become sufficiently large, there is an explosive secondary instability which terminates a simulation. (Numerical computation shows that the lowest eigenvalue of the truncated $\mathbf{K}$ operator becomes negative just before this catastrophe. This eigenvalue is shared by $\delta^2 H$, so the model dynamics suffers from a finite-time singularity.) This limits the ability of the operator expansion algorithm to compute waves close to physical breaking, as described below.

4. Numerical applications

The dynamical model described above has been implemented in a FORTRAN code, handling nonlinearities up to fourth order (fifth-order terms in H) and up to second order in δh. For the computations described below, only first- and second-order nonlinearities were retained, since preliminary tests showed no significant changes when higher orders were included. The dependent variables in the code are the Fourier amplitudes of ζ and ϕ. The code employs periodic boundary conditions, so that the basic operators like $\mathbf{k}^p$ and $(\tanh kh_0)_{\mathrm{op}}$ are multiplicative. Spatial products in the advection terms and in the operator expansion are computed by the pseudospectral method, using fast Fourier transforms and a fully dealiased spatial grid. Time-stepping is handled by a variable-step-size variable-order Adams–Bashforth–Moulton scheme derived from the work of Shampine & Gordon (1975). (I chose this method to minimize time-stepping errors for validation purposes; for most applications a low-order predictor scheme should suffice.) The examples include simulations of harmonic waves, so forcing and damping terms representing an oscillating pressure source and localized friction,

$$f(x) \cos \Omega t - d(x) \phi, \tag{4.1}$$

are added to the right-hand side of (2.2), the Bernoulli equation. The code was written for two horizontal dimensions. The efficiency could be improved for one dimension, or for reflection-symmetric domains, but such optimizations were not implemented for this study. Computations were done on a workstation with typical performance of 50 megaflops. The following examples typically required about 2000 time steps.

One-dimensional computations with 512 Fourier modes each required less than an hour. A two-dimensional computation with 512×256 modes required about 20 hours.

The applications described below all involve depths which are shallow or intermediate compared to the wavelengths. The present algorithm contains the method described by West *et al.* (1987) as a limiting case, so it enjoys the accuracy which they reported for deep-water waves.

4.1. *Interpolation among reference depths*

When the range of depths exceeds about one octave, accuracy is enhanced by using several reference depths, $\{h_j; j = 1, \ldots, N_h\}$, in the leading-order operator $\mathbf{D}_0$, with an interpolation scheme. (The reason behind this is the inadequacy of a first- or second-order Taylor expansion of the hyperbolic tangent over a wide domain.) In the code I have simply used the formula

$$\mathbf{D}_0 f(\boldsymbol{x}) = \left(\frac{[h(\boldsymbol{x}) - h_n]\mathbf{D}_0\{h_{n+1}\}f(\boldsymbol{x}) + [h_{n+1} - h(\boldsymbol{x})]\mathbf{D}_0\{h_n\}f(\boldsymbol{x})}{h_{n+1} - h_n} \right), \tag{4.2}$$

for $\boldsymbol{x}$ such that $h(\boldsymbol{x}) \in [h_n, h_{n+1}]$. The set of reference depths used in the code forms a geometric series with an incremental factor of $\sqrt{2}$, i.e. two values per octave of depth variation. One sees from figure 1 that this ensures that the fractional error in dispersion frequency over a locally flat bottom nowhere exceeds 1%. (It turns out to be computationally preferable to truncate at first order in δh and employ additional depths rather than to retain higher-order terms. Moreover, this avoids difficulties associated with a discontinuous bottom slope. I have performed some computations at $O(\delta h^2)$ for cases like those shown below, but with smooth bottoms. For the mild slopes considered here, the results are barely distinguishable from the first-order ones.)

An interpolation scheme of this sort violates the spirit of the operator expansion itself, in that it uses local operations to approximate intrinsically non-local operators of potential theory. I do not have a formal justification for this approach, but the following applications demonstrate its practical utility.

4.2. *Waves over an underwater bar*

The first example involves time-harmonic waves of moderate amplitude propagating over a bar. Over the bar, the amplitude increases so that bound harmonics are generated; the harmonics propagate freely beyond the bar. In this example, all fields vary in only one horizontal direction (x). Details are taken from Dingemans (1994, 1997), who compares experimental results with several other numerical models. This experiment is particularly difficult to simulate because it includes nonlinear interactions up to the third harmonic and requires accurate propagation of waves in both the shallow and intermediate-depth regimes over a wide range of depths. The bottom geometry, illustrated in figure 2, is given by

$$h(x) = \begin{cases} 0.4 - 0.05(x - 6), & 6 \leqslant x \leqslant 12 \\ 0.1, & 12 \leqslant x \leqslant 14 \\ 0.1 + 0.1(x - 14), & 14 \leqslant x \leqslant 17 \\ 0.4 & \text{elsewhere.} \end{cases} \tag{4.3}$$

All lengths and times here are in Dingemans' scaled units (2 m, $\sqrt{2}$ s) to facilitate comparisons with his work. The experiment was performed under three conditions: A – incident wave period 2.02 and trough-to-crest waveheight 0.02; B – period 2.525 and waveheight 0.029; C – period 1.01 and waveheight 0.041.

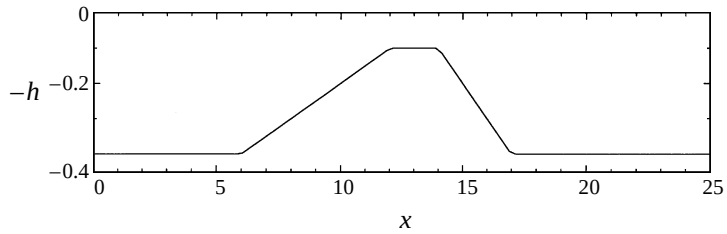

FIGURE 2. Geometry of the bar experiments, after Dingemans (1994).

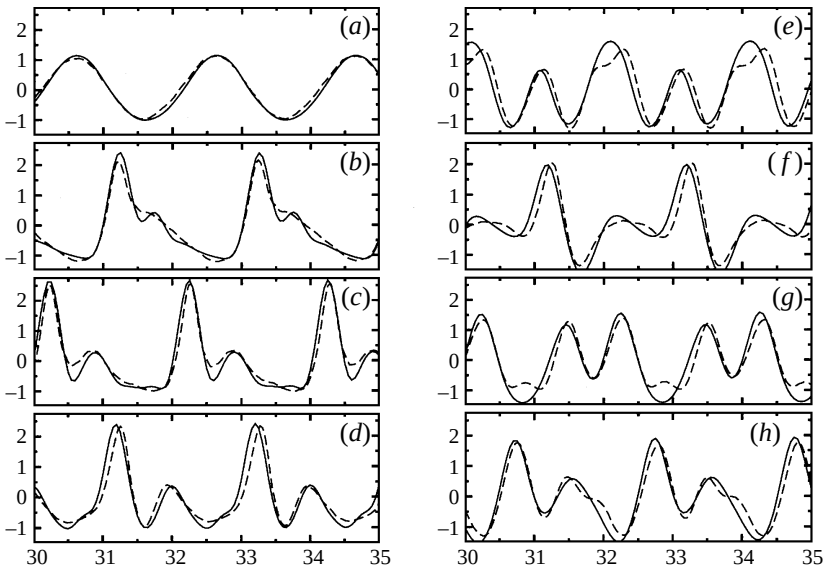

FIGURE 3. Surface height [×100] vs. time (in scaled units) at various locations, for waves over a bar as in an experiment at Delft Hydraulics (Dingemans 1994). Case A: the incident wave period is 2.02, and the waveheight in the region before the bar is 0.02. Solid lines: computed by the present algorithm; dashed lines: experimental data. (*a*) $x = 2$; (*b*) $x = 12.5$; (*c*) $x = 13.5$; (*d*) $x = 14.5$; (*e*) $x = 15.7$; (*f*) $x = 17.3$; (*g*) $x = 19$; (*h*) $x = 21$.

For the numerical model, waves are generated by an oscillating source localized around $x = -4$ and damped by friction acting only in the neighbourhood of $x = 37$. The computational domain had a period of 51.2 units. For conditions A and B, 254 Fourier modes (127 in each direction) were used, with a spatial grid of 512 points. For condition C, 510 modes and 1024 grid points were used.

Time histories of surface height ζ at various locations are shown in figures 3–5. The origin of time for the simulations has been shifted so that the wave crests match the measurements for the gauge at $x = 2$. The small delay between measured and model crests at other locations is a measure of dispersion error in the computation.

The simulations compare well with the experimental measurements in all cases. For condition A, shown in figure 3, the present scheme performs similarly to the Hamiltonian method of Radder (1992), and to a boundary-element model, both shown by Dingemans (1994, 1997). The latter are presumably more accurate than the present model, but are difficult to extend to three-dimensional problems. These three schemes all handle this problem at least as well as Boussinesq-type models, and show similar (so far unexplained) discrepancies from the experiments. The operator

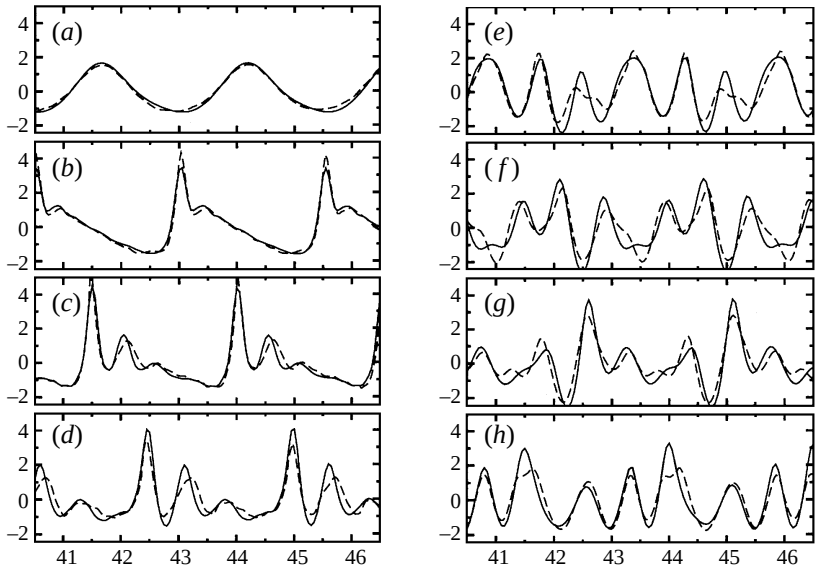

FIGURE 4. As figure 3 but for case B: the incident wave period is 2.525, and the waveheight in the region before the bar is 0.029.

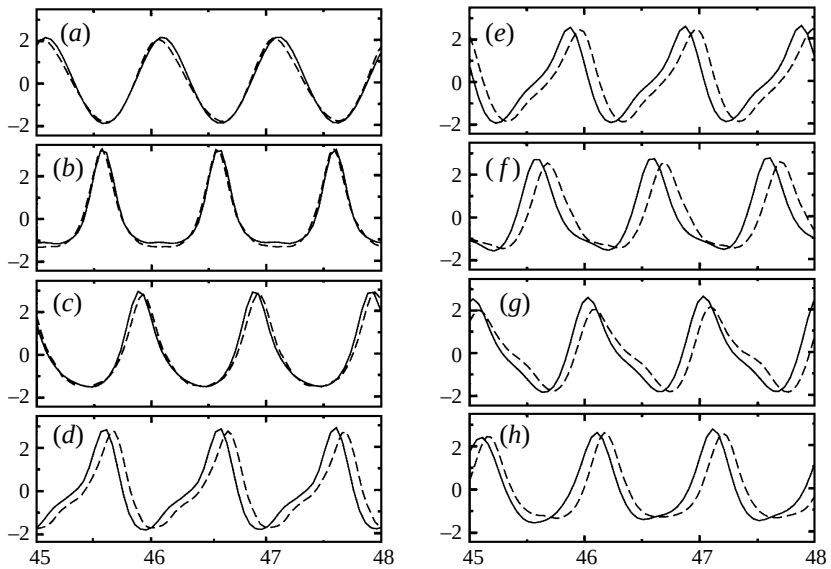

FIGURE 5. As figure 3 but for case C: the incident wave period is 1.01, and the waveheight in the region before the bar is 0.041.

expansion method works well even for case B (figure 4), in which the physical wave forms a spilling breaker over the bar. It also correctly represents the asymmetry of the shorter waves in case C (figure 5), for which Boussinesq-type models are less successful. I have not attempted to model an experimental wavemaker in detail; thus there are small discrepancies in the harmonic content of the incident waves, as may be seen in figures 3(*a*), 4(*a*), and 5(*a*).

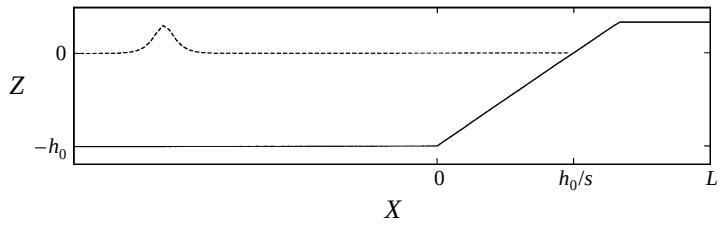

FIGURE 6. Geometry used for the solitary wave computations, after Grilli *et al.* (1994).

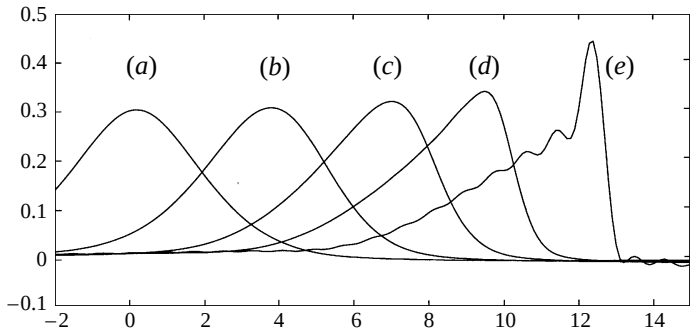

FIGURE 7. Profiles of a solitary wave shoaling on a plane slope. The initial amplitude is $0.3h_0$ and the slope is 1:15, with a toe at $x = 0$. Dimensionless times $t' = t(g/h_0)^{1/2}$: (*a*) 0.2; (*b*) 3.3; (*c*) 6.1; (*d*) 8.3; (*e*) 11.1.

4.3. *Shoaling of solitary waves*

Grilli *et al.* (1994) studied the evolution of solitary waves on sloping plane beaches. They demonstrated the accuracy of a boundary-element potential flow model by comparing its predictions to experimental measurements. Wei *et al.* (1995) tested an extended Boussinesq model of these waves against the same boundary-element model. The geometry of these simulations is shown in figure 6; a flat bottom of depth h_0 is imposed for $x < 0$, and a slope with tangent s for $x > 0$. For the operator expansion the topography is symmetrically extended by reflection through $x = L > 1/s$. Initial conditions are generated as follows. The surface height and potential of a solitary wave are computed by the method of Tanaka (1986). (These waveforms propagate with negligible change in shape according to the operator expansion code with a flat bottom.) The waveform is translated so that the crest is centred at x_c, within the region of uniform depth and such that the initial flow is negligible near the origin and over the slope. The same waveform, reflected through $x = L$, is added to make the potential periodic on a domain of length $2L$. (Thus two solitary waves propagate symmetrically towards an island between them.) No forcing or damping was used in these computations. The geometric series of reference depths was truncated at $h_0/8$, although the domain includes a region with $h \leqslant 0$.

The profiles and shoaling characteristics of solitary waves computed by the operator expansion are quite close to those reported by Grilli *et al.* (1994), until near the time of breaking. Figure 7 shows results for the case of a solitary wave with an initial waveheight of $0.3h_0$ and slope $s = 1/15$. Times are adjusted so the crest passes over the toe of the slope at $t = 0$. (Compare figure 4*a* of Wei *et al.* 1995.) In the last profile shown, one sees that the non-physical small-scale instability described above has arisen; shortly thereafter the numerical derivatives diverge. The time of this profile is

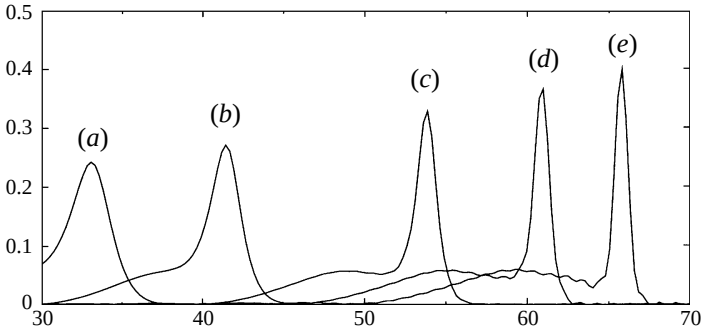

FIGURE 8. Profiles of a solitary wave shoaling on a plane slope. The initial amplitude is $0.2h_0$ and the slope is 1:100, with a toe at $x = 0$. Dimensionless times $t' = t(g/h_0)^{1/2}$: (*a*) 31.3; (*b*) 40.0; (*c*) 53.2; (*d*) 61.1; (*e*) 66.6.

very close to the onset of breaking as observed in the boundary element computation and the experiment. For steeper slopes, when there is significant runup, the operator expansion sometimes exhibits other spurious instabilities; the explanation and possible remedies for these await further study.

Figure 8 shows results of a computation with initial waveheight of $0.2h_0$ and slope $s = 1/100$. (Compare figure 4*a* of Wei *et al.* 1995.) Again, the last profile shown corresponds to a time near the breaking point. In this case, the operator-expansion computation is smooth until somewhat later than the onset of breaking in the boundary-element code; the waveform becomes progressively sharper, but its height does not increase significantly. This result differs from the extended Boussinesq model of Wei *et al.* (1995), which overshoals before the breaking point.

4.4. *Diffraction by a shoal*

The next application involves two horizontal dimensions; this experiment has been used to validate diffraction models such as the mild-slope equation. Berkhoff, Booij & Radder 1982 generated time-harmonic waves propagating at an oblique incidence angle over a sloping plane surmounted by an ellipsoidal shoal. The range of depths is similar to that of the bar experiment discussed above, so we expect the second harmonic to attain a significant amplitude. (Temporal information was not reported by Berkhoff *et al.*)

The depth is given in a coordinate system (x', y'), rotated by 20° from the (x, y) coordinates of the simulation:

$$h(\boldsymbol{x}) = \begin{cases} 0.45 - 0.02(y' + 5.84) - d(x', y') & \text{if } y' > -5.84 \\ 0.45 & \text{otherwise.} \end{cases} \tag{4.4}$$

The shoal thickness d is given by

$$d(x', y') = \begin{cases} -0.3 + 0.5[1 - (x'/5)^2 - (y'/3.75)]^{1/2} & \text{if } (x'/4)^2 + (y'/3)^2 < 1 \\ 0 & \text{otherwise.} \end{cases} \tag{4.5}$$

All lengths here are in metres. Figure 9 illustrates the bottom topography. (The orientation has been changed from the experimental coordinates so that waves propagate in the positive y-direction.) The incident waves had a period of 1 s and waveheight of 4.64 cm in the deep-water region.

For the simulation, the measurement geometry was embedded in a periodic domain 40 m by 44.4 m in extent. The topography given by (4.4) was used for $x \in [0, 20]$ m

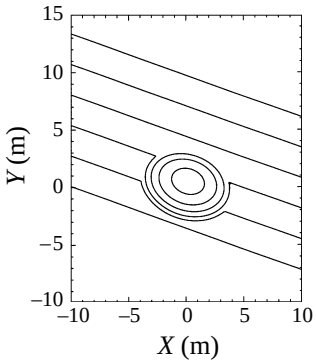

FIGURE 9. Geometry of the shoal experiment, after Berkhoff *et al.* (1982). Depth contours range from 0.15 (at top of figure) to 0.4 m (at bottom) at intervals of 0.05 m.

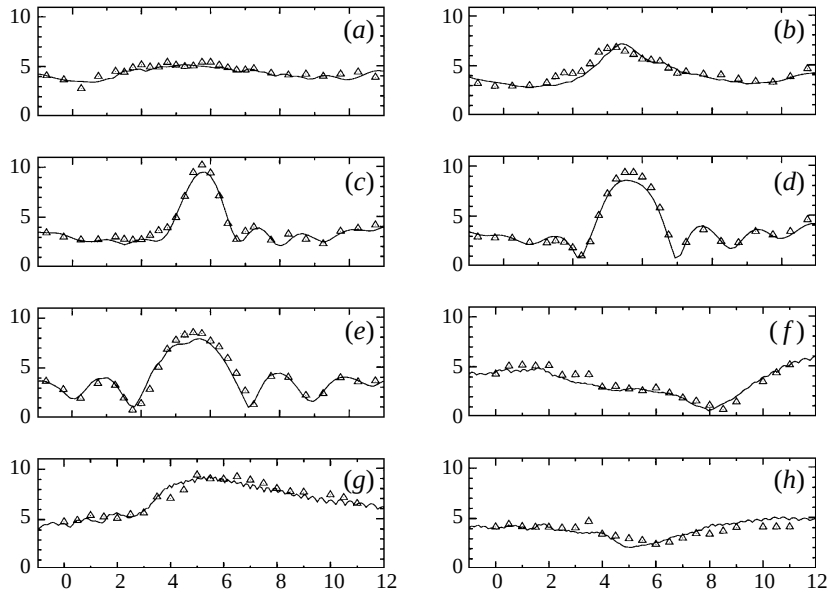

FIGURE 10. Waveheight (cm) vs. location (m) along transects of the measurement area in the shoal experiment (Berkhoff *et al.* 1982). Solid lines: computed by the present algorithm; △: experimental data. Locations of transects: (*a*) $y = 1$ m; (*b*) $y = 3$ m; (*c*) $y = 5$ m; (*d*) $y = 7$ m; (*e*) $y = 9$ m; (*f*) $x = 2$ m; (*g*) $x = 0$ m; (*h*) $x = -2$ m.

and for $y \in [-10, 15]$ m such that $h \geqslant 0.1$ m. This was extended with a flat region to $y = 20$ m and a plane sloping from 0.1 m to 0.45 m, between $y = 20$ and $y = 30$ m. The depth field was finally reflected across the line $x = 20$ m, effectively imposing reflecting sidewall boundary conditions. Other simulations have shown that such differences do not substantially change the waveheight in the measurement region. An oscillating pressure source was located at $y = -12.4$ m, and friction was applied in the neighbourhood of $y = 23$ m. Waveheights measured along various transects in the experiment are compared with simulation results in figure 10. Overall the shoaling and diffraction effects are modelled well by the operator expansion method. The amplitudes in the focal region are slightly lower than in the experiment. Figure 11 depicts the surface elevation at the end of the simulation. The pattern of interference

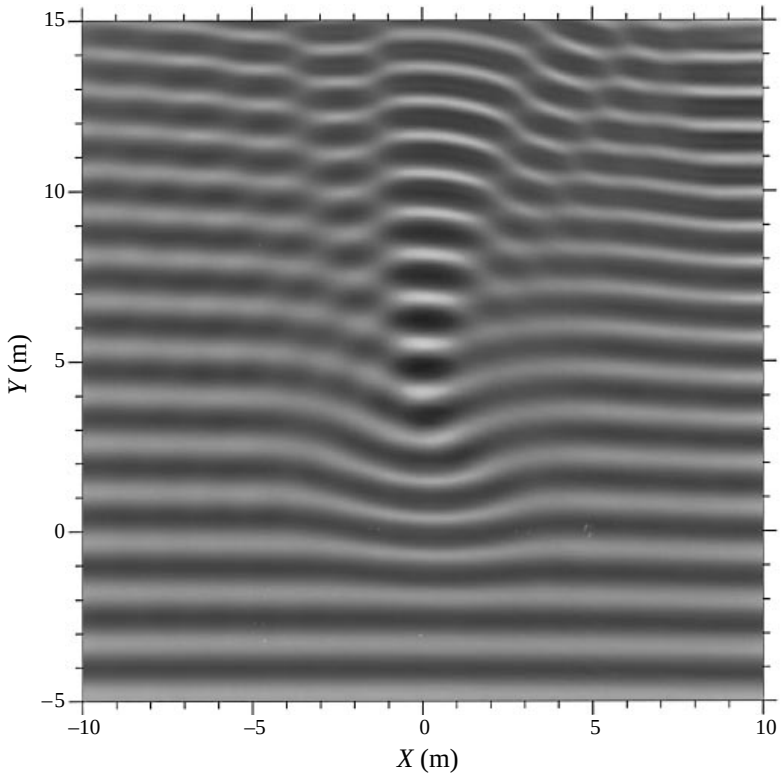

FIGURE 11. Surface elevation in the shoal experiment, as computed by the present algorithm. Brightness is proportional to instantaneous height above the minimum.

fringes and sharpened wave crests is quite similar to the one photographed by Berkhoff *et al.*

5. Discussion

We have seen that the operator-expansion formalism allows faithful computations of surface waves over variable depth. It handles diffraction and nonlinear effects on shoaling and dispersion with accuracy similar to that of extended Boussinesq models, without the long-wave approximation. A numerical implementation is not as robust as boundary-element methods (e.g. it sometimes suffers from non-physical short-wavelength instabilities, and the operator expansion itself does not converge for large slopes), but is less demanding of computational resources, especially for problems involving two horizontal dimensions. (The operation count is proportional to $N \log N$ where N is the number of grid points or wavenumbers, and the storage requirements are proportional to N, whereas boundary-element methods require solution of a dense $O(N)$ matrix problem at every time step.) It may be possible to handle breaking waves and runup within this formulation by use of methods like those described by Kirby (1997) and Dingemans (1997). Effects of surface tension can be incorporated easily, as discussed by Milder (1990).

This work was supported in part by the US Office of Naval Research, Sensing and Systems Division. I am indebted to Dr D. M. Milder for numerous conversations,

and in particular for the suggestion to use multiple reference depths. A deep-water simulation code written by Drs H. T. Sharp and D. M. Milder served as a prototype for the code employed in this work. Dr K. Apfeldorf collaborated in preliminary work on the variable depth problem. Dr M. W. Dingemans kindly provided the data from the Delft bar experiments. I am grateful to an anonymous reviewer for several corrections and for bringing the work of Craig and associates to my attention.

Appendix. Relation to the formalism of Craig & Sulem

The operator $\mathbf{K}$ associated with the kinetic energy in the Hamiltonian (2.3) is called the Dirichlet–Neumann operator by Craig & Sulem (1993). They expand it in orders of ζ to obtain a dynamical model for two-dimensional waves over uniform depth. By substituting the expansion (2.25) into (2.4) we obtain

$$\mathbf{K}\phi \sim \mathbf{k}\mathbf{H}'\phi + [\zeta\mathbf{k}^2 - \mathbf{k}\mathbf{H}'\zeta\mathbf{k}\mathbf{H}']\phi + [-\zeta\mathbf{k}^2\zeta\mathbf{k}\mathbf{H}' - \tfrac{1}{2}\mathbf{k}\mathbf{H}'\zeta^2\mathbf{k}^2 + \tfrac{1}{2}\zeta^2\mathbf{k}^3\mathbf{H}' + \mathbf{k}\mathbf{H}'(\zeta\mathbf{k}\mathbf{H}')^2]\phi + (\nabla\zeta)^2\mathbf{k}\mathbf{H}'\phi - \nabla\zeta\cdot\nabla\phi. \tag{A 1}$$

For fields varying in only one horizontal dimension, the $\mathbf{k}$ operator is equivalent to $-\mathrm{i}\nabla$, which obeys the derivative product rule. After a few lines of algebra we find that the second-order truncation of $\mathbf{K}\phi$ in this case is equal to

$$\mathbf{K}_1\phi = \mathbf{k}\mathbf{H}'\phi + \mathbf{k}\zeta\mathbf{k}\phi - \mathbf{k}\mathbf{H}'\zeta\mathbf{k}\mathbf{H}'\phi - \tfrac{1}{2}\mathbf{k}^2\zeta^2\mathbf{k}\mathbf{H}'\phi - \tfrac{1}{2}\mathbf{k}\mathbf{H}'\zeta^2k^2\phi + \mathbf{k}\mathbf{H}'\zeta\mathbf{k}\mathbf{H}'\zeta\mathbf{k}\mathbf{H}'\phi. \tag{A 2}$$

For uniform depth h_0, the $\mathbf{H}'$ operator reduces to $(\tanh kh_0)_{\mathrm{op}}$, and then $\mathbf{K}_1$ is identical to the truncated Dirichlet–Neumann operator $G_0 + G_1 + G_2$ of Craig & Sulem (1993). Similar use of the product rule verifies the equivalence of their equations of motion to (2.1), (2.2) above, under the same restrictions.

REFERENCES

Berkhoff, J. C. W., Booij, N. & Radder, A. C. 1982 Verification of numerical wave propagation models for simple harmonic linear water waves. *Coastal Engng* **6**, 255–279.

Broer, J. L. F. 1974 On the Hamiltonian theory of surface waves. *Appl. Sci. Res.* **29**, 430–446.

Choi, W. 1995 Nonlinear evolution equations for two-dimensional surface waves in a fluid of finite depth. *J. Fluid Mech.* **295**, 381–394.

Craig, W. & Groves, M. D. 1994 Hamiltonian long-wave approximations to the water-wave problem. *Wave Motion* **19**, 367–389.

Craig, W. & Sulem, C. 1993 Numerical simulation of gravity waves. *J. Comput. Phys.* **108**, 73–83.

Dingemans, M. W. 1994 Comparison of computations with Boussinesq-like models and laboratory measurements. *Rep.* H1684.12, Delft Hydraulics.

Dingemans, M. W. 1997 *Water Wave Propagation over Uneven Bottoms*. World Scientific.

Grilli, S. T., Subramanya, R., Svendsen, I. A. & Veeramony, J. 1994 Shoaling of solitary waves on plane beaches. *J. Waterway Port Coastal Ocean Engng* **120**, 609–628.

Kirby, J. T. 1997 Nonlinear, dispersive long waves in water of variable depth. In *Gravity Waves in Water of Finite Depth* (ed. J. N. Hunt). Advances in Fluid Mechanics, vol. 10, pp. 55–125. Computational Mechanics.

Mei, C. C. & Liu, P. L.-F. 1993 Surface waves and coastal dynamics. *Ann. Rev. Fluid Mech.* **25**, 215–240.

Milder, D. M. 1977 A note regarding 'On Hamilton's principle for surface waves.' *J. Fluid Mech.* **83**, 159–161.

Milder, D. M. 1990 The effects of truncation on surface-wave Hamiltonians. *J. Fluid Mech.* **217**, 249–262.

Milder, D. M. 1996 Role of the admittance operator in rough-surface scattering. *J. Acoust. Soc. Am.* **100**, 759–768.

Miles, J. W. 1977 On Hamilton's principle for surface waves. *J. Fluid Mech.* **83**, 153–158.

Mooiman, J. 1991 Boussinesq equations based on a positive definite Hamiltonian. *Rep.* Z294, Delft Hydraulics.

Radder, A. C. 1992 An explicit Hamiltonian formulation of surface waves in water of finite depth. *J. Fluid Mech.* **237**, 435–455.

Shampine, L. F. & Gordon, M. K. 1975 *Computer Solution of Ordinary Differential Equations*. W.H. Freeman.

Tanaka, M. 1986 The stability of solitary waves. *Phys. Fluids* **29**, 650–655.

Watson, K. M. & West, B. J. 1975 A transport-equation description of nonlinear ocean surface wave interactions. *J. Fluid Mech.* **70**, 815–826.

Wei, G., Kirby, J. T., Grilli, S. T. & Subramanya, R. 1995 A fully nonlinear Boussinesq model for surface waves. Part 1. Highly nonlinear unsteady waves. *J. Fluid Mech.* **294**, 71–92.

West, B. J., Brueckner, K. A., Janda, R. S., Milder, D. M. & Milton, R. L. 1987 A new numerical method for surface hydrodynamics. *J. Geophys. Res.* **92**, 11803–11824.

Wright, J. & Creamer, D. B. 1994 Improved linear representation of surface waves. Part 2. Slowly varying bottoms and currents. *J. Fluid Mech.* **261**, 65–74.

Yoon, S. B. & Liu, P. L.-F. 1994 A note on Hamiltonian for long water waves in varying depth. *Wave Motion* **20**, 359–370.

Zakharov, V. E. 1968 Stability of periodic waves of finite amplitude on the surface of a deep fluid. *J. Appl. Mech. Tech. Phys.* **2**, 190–194.